Available online at www.sciencedirect.com
SCIENCE DIRECT®
Polymer 44 (2003) 6781–6787
polymer
www.elsevier.com/locate/polymer

Structure evolution in melt crystallised PEEK

M.J. Jenkins[a,*], J.N. Hay[a], N.J. Terrill[b]

[a]*Metallurgy and Materials, School of Engineering, University of Birmingham, Birmingham B15 2TT, UK*
[b]*CLRC Daresbury Laboratory, Warrington, Cheshire WA4 4AD, UK*

Received 24 February 2003; received in revised form 30 July 2003; accepted 4 August 2003

Abstract

The melt crystallisation of PEEK has been analysed using dynamic small and wide angle scattering, in addition, differential scanning calorimetry has also been used. The crystallisation data have been analysed in terms of the Avrami, Hoffman–Lauritzen and Cahn–Hilliard models. The mechanistic n values, nucleation constant, K_g, and the effective diffusion co-efficient for the crystallisation of PEEK in the temperature range 290–320 °C are reported. These results are discussed in terms of the level of insight they give into the nucleation process.

Keywords: PEEK; Small angle X-ray; Wide angle X-ray

1. Introduction

Cooling a crystallisable polymer from a temperature above the melting point can result in the formation of crystallites. The kinetics of phase change during crystallisation can be described using the Avrami model. This approach has been highly successful in describing crystallisation in polymers [1,2]. The model relates the extent of crystallinity to time, such that,

$$X(t) = 1 - \exp(zt^n) \tag{1}$$

where z is related to the rate of phase change and n is a mechanistic constant. Values of between 3 and 4 are common for polymers, indicating either pre-determined or sporadic growth spherulitic crystallites. The growth rate of crystals and the dependence on temperature was later described by Turnbull and Fisher [3].

$$g = g_0 \exp\left(-\frac{\Delta E_{act}}{RT}\right)\exp\left(\frac{\Delta f G^*}{RT}\right) \tag{2}$$

where g_0 is constant, ΔE_{act} is the activation energy of viscous flow and $\Delta f G^*$ is the free energy of formation of the critical size nucleus. As the temperature approaches the glass transition, the first term in the above equation is dominant and the rate-determining step is the diffusion of chains to the growth face. As the temperature approaches the melting point, the rate-determining step is nucleation controlled and the second term becomes dominant. The opposing temperature dependencies of the two exponential terms results in a peak in the plot of growth rate against temperature.

For homogeneous sporadic nucleation, the nucleation rate is related to temperature by the following expression, [3]

$$N = N_0 \exp\left(-\frac{E_D}{kT} - \frac{\Delta G^*}{kT}\right) \tag{3}$$

where E_D is the activation energy for transport across the surface of the nucleus, ΔG^* is the free-energy of formation of the critical size nucleus.

This model was later refined by Hoffman and Lauritzen [4] to describe polymer crystallisation by the introduction of a modified nucleation term. In this modification, three regimes of nucleation are possible, each regime predominating at different temperatures. At temperatures approaching the melting point, each nucleation on the growing crystal surface leads to rapid completion of the growth strip by chain folding prior to the next nucleation event, this is referred to as regime I. At much lower temperatures there is prolific multiple nucleation on the growth surface and this is referred to as regime III. Between these two limits there is competition between chain folding and nucleation, growth in this region is termed regime II.

* Corresponding author. Tel.: +44-121-414-2841; fax: +44-121-414-5232.
E-mail address: m.j.jenkins@bham.ac.uk (M.J. Jenkins).

0032-3861/$ - see front matter © 2003 Elsevier Ltd. All rights reserved.
doi:10.1016/S0032-3861(03)00749-3

A recent development in the description of nucleation mechanisms has been initiated from the observation of small angle X-ray (SAX) scattering before wide angle X-ray (WAX) scattering in the crystallisation of polypropylene [5]. The development of the SAX prior to WAX has been found to grow exponentially with time and has been fitted to the Cahn–Hilliard theory for spinodal decomposition. The SAX peak has also been found to move to smaller angles with time, stopping when WAX is observed. There is evidence of large-scale structure in SAX before WAX and this has been interpreted as pre-crystallisation density fluctuations, originating from conformational changes within the polymer chains [6].

The appearance of SAX before WAX has also been reported in other polymers such as PEEK [7]. The study has focused on cold crystallisation of the amorphous material by heating to the crystallisation temperature from below the glass transition temperature. The observed development of SAX scattering before WAX is interpreted as the formation of long-range nanostructures and is discussed in terms of the spinodal assisted nucleation concept. The aim of this paper is therefore to establish whether SAX develops prior to WAX in melt crystallised PEEK. The evolution of any structure in SAX scattering will be considered in terms of the models discussed above, comparisons between the theories will be made.

2. Experimental

2.1. Materials

Thin films of PEEK were supplied by ICI Ltd. Thicknesses were 250 μm. Sheets of clear scratch free mica were supplied by the Attwater Group.

Dynamic SAX/WAX measurements were made on beamline 8.2 of the SRS at the CCLRC Daresbury Laboratory, UK using a camera length of 3.5 m. The main details of the station geometry and data acquisition electronics have been given in elsewhere [7]. The station delivers 4×10^{10} photons/s of monochromatic X-rays (1.52 Å) in a 3 mm × 0.5 mm focussed spot. The scattering patterns were collected using a delay line quadrant detector (SAXS [8]) and a curved linear detector from INEL (WAXS [9]).

Circular samples of PEEK were pressed from thin films using a 5 mm diameter hole punch and the samples were mounted between two circular samples of mica. The resulting structure was then placed on a DSC pan (TA Instruments) and sealed. A circular section was removed from the DSC pan and lid to enable the transmission of the X-ray beam. A Linkam hot stage DSC was used to control the sample temperature. The base of the DSC cell was drilled to allow the X-ray beam to pass through the sample. The temperature was calibrated using the melting points of tin and indium.

The procedure adopted for all the experiments was as follows: samples were heated to 350 °C at 10 °C min^{-1} to melt the crystallites. Samples were subsequently cooled to the crystallisation temperature as rapidly as possible whilst maintaining control of the DSC cell. The maximum cooling rate was found to be 50 °C min^{-1}. Time resolved SAX and WAX scattering data were then recorded during the subsequent re-crystallisation from the melt.

The SAX and WAX data were normalised for beam decay and detector variation using OTOKO [10]. A scattering pattern from wet collagen (rat-tail) was used for calibration of the q scale. HDPE was used for the 2θ calibration.

The peak intensity and area in the SAX scattering traces and the intensity of the 110 peak in the WAX scattering were measured using a Microsoft Excel macro routine. The SAX peak data were used in the measurement of the crystallisation half time and also in an Avrami analysis, in which the extent of crystallinity, Xt, was defined as,

$$Xt = \frac{I_\infty - I_t}{I_\infty - I_0} \tag{4}$$

where I_t is the intensity at time t and I_0 and I_∞ are the intensities at the beginning and end of the crystallisation process. Therefore, a plot of $\log[-\ln(Xt)]$ against $\log t$ will give a line of slope n and intercept $\log z$.

The crystallisation of PEEK was also measured using a Perkin–Elmer differential scanning calorimeter, model DSC 2B which was interfaced to a personal microcomputer. The thermal response of the instrument was calibrated from the enthalpy of fusion of a known mass of indium (99.999% pure). The temperature scale of the calorimeter was calibrated using the melting points of indium, tin and lead. Plots of actual against experimental melting points were linear and used to calibrate the calorimeter temperature directly after correcting for thermal lag. Corrections were made for thermal lag by extrapolation to zero heating rate.

Samples in the form of discs (1 mm thick and 3 mm in diameter) were contained within aluminium pans, and an empty pan was used as a reference. The samples were first heated to 380 °C and held at this temperature for 1 min, then cooled rapidly to the crystallisation temperature and maintained at this temperature until the DSC trace returned to the calorimeter baseline.

3. Results and discussion

The development of SAX and WAX scattering with time during a melt crystallisation at 290 °C are shown in Figs. 1 and 2, respectively. Fig. 1 shows the development of a peak centred at a scattering vector of 0.031 nm^{-1}, which continues to grow with time until a maximum is reached at 250 s. However, the location of the peak does not appear to change over the duration of the experiment. Fig. 2 shows the development of the Bragg peaks in the WAX scattering.

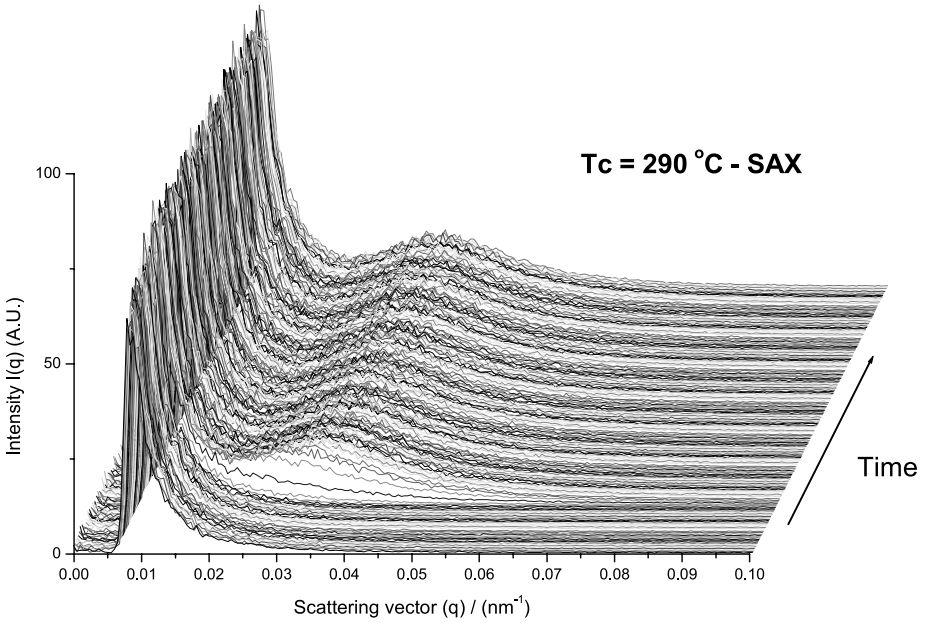

Fig. 1. Development of SAX scattering with time at a crystallisation temperature of 290 °C.

The crystallisation half times were measured using both DSC and SAX scattering and the variation with crystallisation temperature is shown in Fig. 3. The half times measured using DSC exhibit a similar temperature dependence to those measured using SAX scattering. This indicates that the SAX scattering develops on a timescale similar to that observed using calorimetry. The increase in crystallisation half time with decreasing supercooling can be explained in terms of the competition between nucleation and growth, as described by Turnbull and Fisher. The crystallisation process is controlled by the nucleation density at temperatures approaching the melting point and by the diffusion of chains to the crystal growth face at temperatures approaching the glass transition. Competition between the two factors results in a minimum in the crystallisation half life approximately midway between the melting point and the glass transition.

Treatment of crystallisation data using the Avrami approach can provide additional insight into the crystallisation mechanism. Fig. 4 shows an Avrami plot for a crystallisation temperature of 310 °C. The Avrami plot exhibits a linear section over which the mechanistic n value can be calculated, the n values are shown in Table 1. Overall, the most probable mechanism is that of

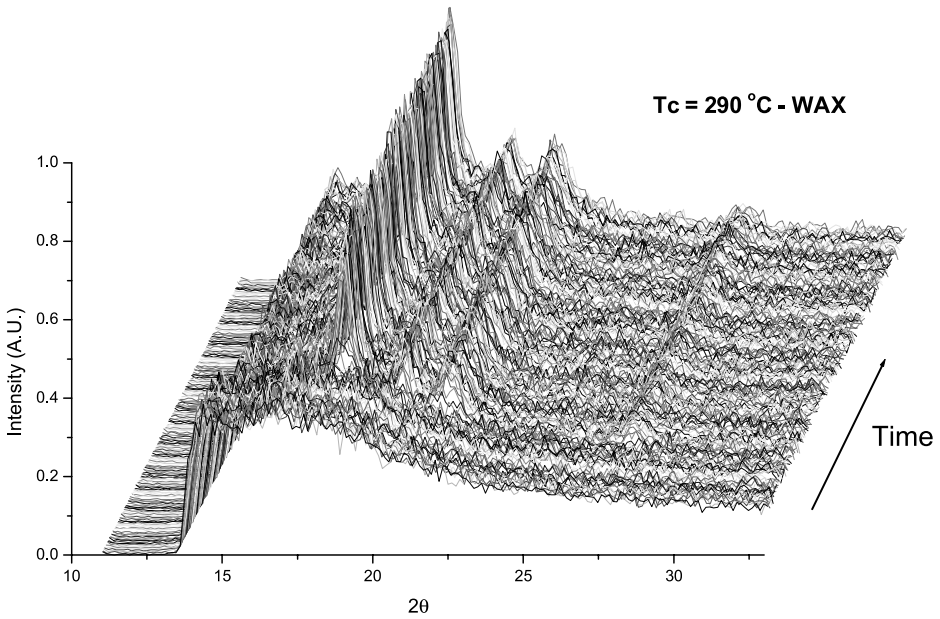

Fig. 2. Development of WAX scattering with time at a crystallisation temperature of 290 °C.

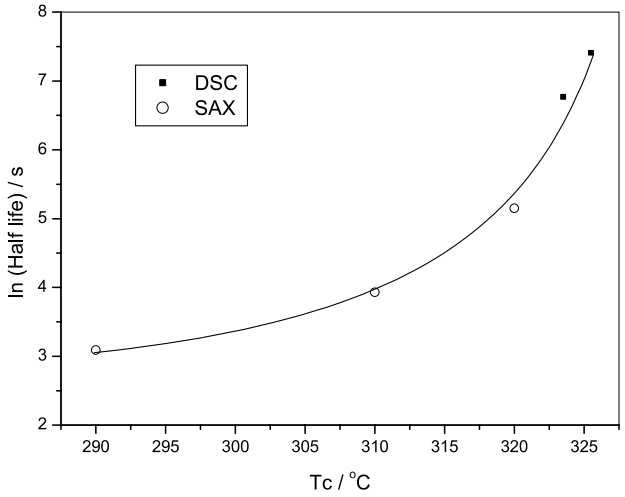

Fig. 3. Variation of half life with crystallisation temperature as measured by DSC and SAX scattering.

predetermined nucleation of spherulitic crystallites. Although successful in describing the growth of crystallites, the Avrami approach does not provide significant insight into the nucleation process.

3.1. Hoffman and Lauritzen model

More insight into the possible nucleation mechanism can be found using the Hoffman and Lauritzen approach. In this model the relationship between the linear growth rate and the supercooling, ΔT, is given by,

$$\mathrm{Gr} = G_0 \exp\left(-\frac{U^*/R}{T - T_\infty}\right)\exp\left(\frac{K_g}{T\Delta T f}\right) \quad (5)$$

The first term describes the increased melt viscosity and reduced molecular mobility as the temperature approaches the equilibrium temperature T_∞ where molecular motion due to viscous flow ceases. This temperature is assumed to be 30 K below the glass transition temperature. U^* is the activation energy for segmental jumps that Hoffman has assigned a value of 6300 J/mol.

The second term accounts for the effect of primary nucleation on the crystallisation and is dominant at low degrees of supercooling, $\Delta T = T_m^0 - T$, where T_m^0 is the equilibrium melting point. The parameter $f = 2T/(T + T_m^0)$ is a correction factor which accounts for the change in the latent heat of fusion that occurs with reduced crystallisation temperatures.

The nucleation constant K_g is dependent on the surface free energy of the crystals and the heat of fusion and for

Table 1
Kinetic parameters obtained from SAX scattering

Temperature (°C)	Avrami n value	Cahn–Hilliard D_{eff} (Å^2 s^{-1}
290	3.21	2.502
310	2.15	2.02
320	1.77	2.82

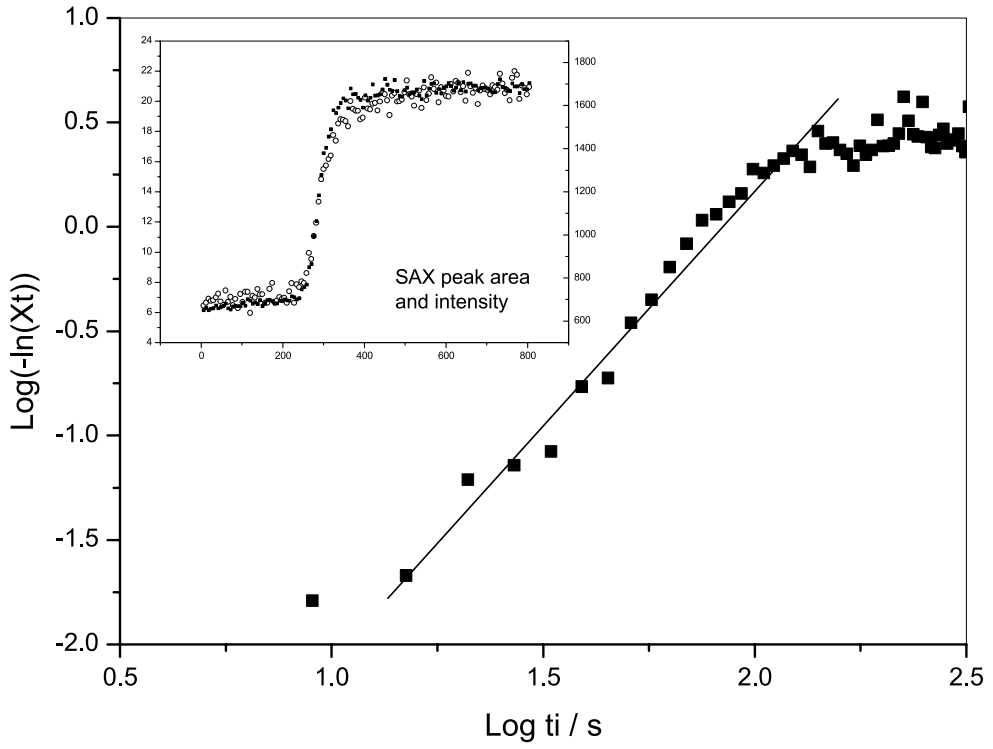

Fig. 4. Avrami plot for a crystallisation temperature of 290 °C.

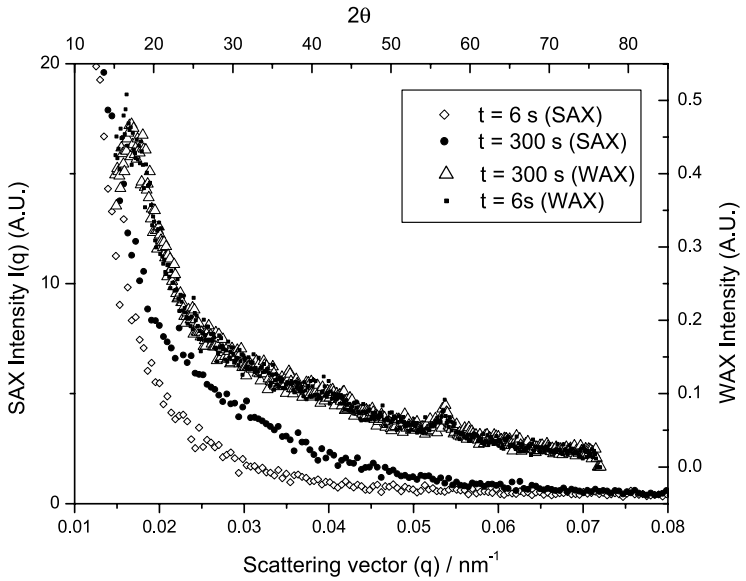

Fig. 5. SAX and WAX scattering traces for times of 6 and 300 s.

regime III is defined by,

$$K_g = \frac{4b_0\sigma\sigma_e T_m^0}{\Delta H_f k} \quad (6)$$

where b_0 is the distance between two adjacent fold planes which in the case of PEEK is 0.592 nm [11], σ and σ_e are the surface free energies per unit area of the crystalline lamellae that run parallel and perpendicular to the chain direction, respectively. ΔH_f is the heat of fusion per unit volume and k is the Boltzmann constant. The heat of fusion of PEEK was taken as 122.5 J/g [12].

The above equation has been modified such that the growth rate has been replaced by the reciprocal of the crystallisation half life. This enables the nucleation constant to be found from plots of $\ln(1/t_{0.5}) + U^*/[R(T - T_\infty)]$ against $1/(T/\Delta Tf)$, the slope of the line being the nucleation constant K_g. Analysis of the early stages of SAX scattering data using the Hoffman and Lauritzen approach gives a nucleation constant of -6.8×10^5. It is clear that a transition from one regime to another did not occur in the temperature range studied, but as the grade of PEEK under investigation contains a high level of added nucleating agent and crystallisation occurred mainly at high supercoolings the mechanism is probably that of regime III, in which there is prolific multiple secondary nucleation.

3.2. Cahn–Hilliard approach

Inspection of the SAX scattering traces shown in Fig. 1 at the point when peaks begin to appear in the WAX scattering traces (Fig. 2) shows that a peak is already evident in the SAX. The observation is illustrated more clearly for a crystallisation temperature of 310 °C. Fig. 5 shows SAX and WAX scattering traces for time periods of 6 and 300 s, it is clear that at a crystallisation time of 300 s, there is no evidence for the formation of Bragg peaks in the WAX trace, whereas in the SAX scattering, a peak is seen to have developed.

Fig. 6 shows the variation of induction time with crystallisation temperature for both SAX and WAX. The observed increase is characteristic of the nucleation control at temperatures approaching the melting point, with the decrease in nucleation density resulting in an increased induction time. Further insight is gained when the respective SAX and WAX induction times are considered. It is again clear that SAX develops prior to WAX, but it is also apparent that the difference between the induction times measured using the respective techniques increases as the crystallisation temperature approaches the melting point, with the induction time observed in WAX increasing more rapidly with increasing temperature in comparison to that observed in SAX scattering.

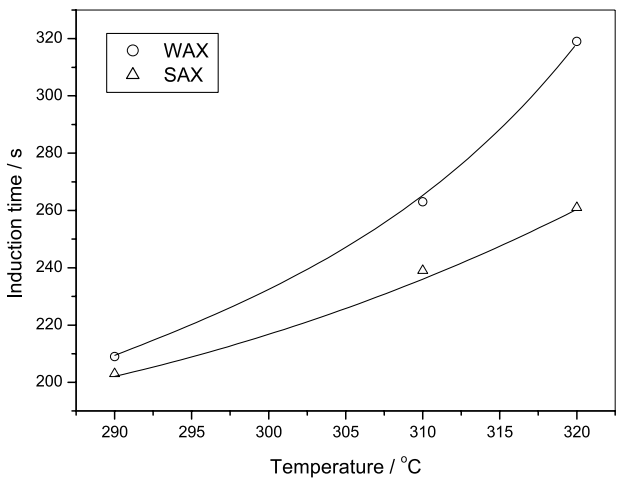

Fig. 6. Variation for the induction time for crystallisation as measured by SAX and WAX.

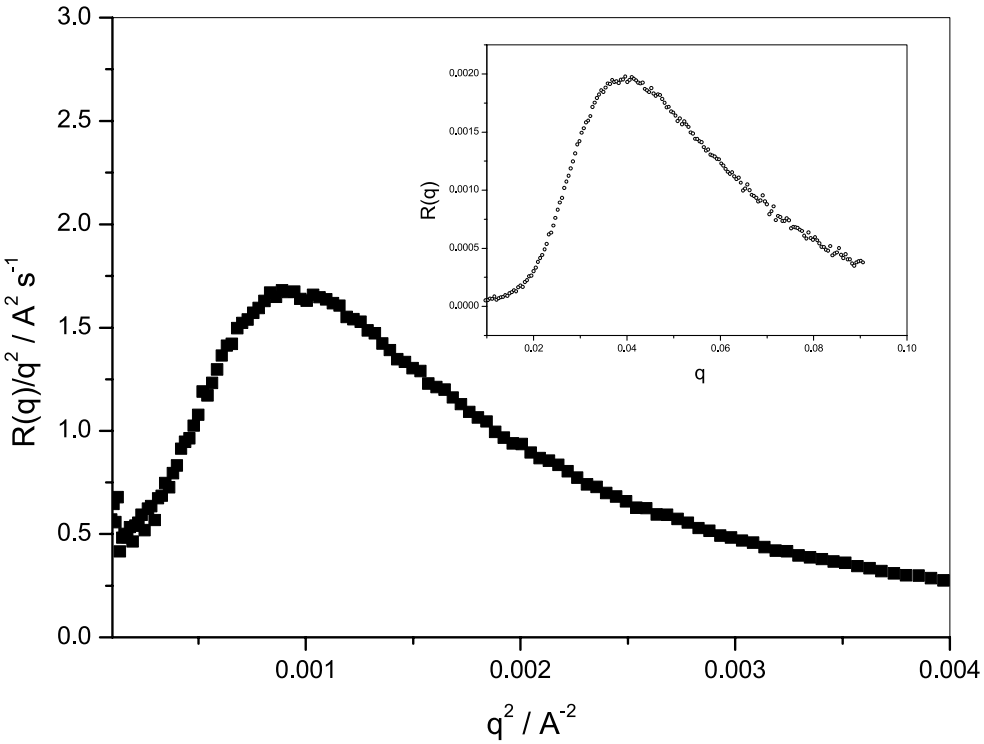

Fig. 7. Cahn–Hilliard plot for SAX data in the time period where no WAX was observed. Crystallisation temperature of 290 °C.

The appearance of SAX during the induction times observed in WAX has been attributed to the formation of long range density fluctuations and a corresponding pre-crystallisation ordering [13,14]. As a result, the trend observed in the induction times measured in SAX and WAX scattering suggest that the ordering phenomena become increasingly important as the crystallisation temperature increases and the nucleation density decreases.

The linearised theory of spinodal decomposition relates the scattered intensity with time according to the following relation,

$$I(q,t) = I(q,0)\exp[2R(q)t] \tag{7}$$

where $R(q) \propto q^2(1 - Bq^2)$ with B a positive constant. $R(q)$ is further controlled by the transport properties,

$$D_{\text{eff}} = -\frac{2R(q)}{q^2} \text{ as } q \text{ tends to zero.} \tag{8}$$

The effective diffusion constant, D_{eff}, can be determined from an extrapolation to $q = 0$ of the linear section of $R(q)/q^2$ during the phase change.

Therefore, if a spinodal decomposition process occurs, a plot of $R(q)/q^2$ versus q^2 should be linear over a low scattering vector range with a negative slope. The intercept from this linear range gives the effective diffusion coefficient (D_{eff}). Treatment of the SAX scattering data over the WAX induction time using the Cahn–Hilliard approach shows a good fit to the model over the q range 0.035–0.045. This is shown in Fig. 7. Although the effective diffusion coefficient (D_{eff}) obtained for the crystallisation temperatures revealed no trend, the magnitudes of the measured D_{eff} values (2.02–2.8 $\text{Å}^2\,\text{s}^{-1}$) are in agreement with other reported data on iPP, HDPE and PET [6].

4. Conclusions

Crystallisation data can be treated using a range of models. The Avrami approach when applied to melt crystallisation data obtained for PEEK provides an insight into the crystallisation mechanism. This has been found to be the predetermined nucleation of either spherulitic or disc like crystallites. Although successful in describing the development of crystallites, the approach provides limited insight into the nucleation mechanism. The nucleation process can be described in more detail by using the Hoffman and Lauritzen approach. The supercoolings adopted in this study indicate a regime III nucleation process, which involves prolific multiple nucleation on the growth surface (not unlikely in a system with many nucleating agents in it).

An alternative description of crystallisation derives from the Cahn–Hilliard approach, as recently developed by Ryan et al. [5,6,15] The basis of the approach is a pre-nucleation density fluctuation that is driven by conformational change. Application of the theory to the melt crystallisation of PEEK shows a linear dependence of $R(q)/q^2$ on q^2, giving an effective diffusion constant of approximately 2, which is in good agreement with previous studies on other polymers. These results suggest that the Cahn–Hilliard approach can

be applied to the melt crystallisation of PEEK. However, the conformational changes that supposed to drive the pre-crystallisation density fluctuation require further experimental verification.

References

[1] Hay JN. Br Polym J 1971;3:74–82.
[2] Hay JN. In: Miller RL, editor. New York: Gordon Breach Science Publishers Ltd, 1979.
[3] Turnbull D, Fisher JC. J Chem Phys 1949;17:71.
[4] Hoffman JD, Lauritzen JI. J Appl Phys 1973;44:4340.
[5] Terrill NJ, Fairclough PA, Towns-Andrews E, Komanschek BU, Young RJ, Ryan AJ. Polymer 1998;39(11):2381–5.
[6] Ryan AJ, Fairclough PA, Terrill NJ, Olmsted PD, Poon CK. Faraday Discuss 1999;112:13–29.
[7] Bras W, Derbyshire GE, Ryan AJ, Mant GR, Felton A, Lewis RA, Hall CJ, Greaves GN. Nucl Instrum Methods Phys Res 1993;A326:587.
[8] Lewis RA, Sumner I, Berry A, Bordas J, Gabriel A, Mant G, Parker B, Roberts K, Worgan J. Nucl Instrum Methods Phys Res 1988;A273:773.
[9] Ballon J, Comparat V, Pouxe J. Nucl Instrum Methods Phys Res 1983;217:216.
[10] http://www.srs.dl.ac.uk/ncd/computing/manual.otoko.html.
[11] Nogales A, Ezquerra TA, Denchev FJ, Balta-Calleja FJ. Polymer 2001;42:5711–5.
[12] Hay JN, Kemmish DJ, Langford JI, Rae AIM. Polym Commun 1984;25:175.
[13] Mehmet-Alkan AA, Hay JN. Polymer 1993;34:3529.
[14] Ezquerra TA, Lopez-Cabaros E, Hsio BS, Balta-Calleja FJ. Phys Rev E 1996;54:989.
[15] Olmstead PD, Poon WC, McLeish TCB, Terrill NJ, Ryan AJ. Phys Rev Lett 1998;81:373.